High-resolution Hyperspectral Image Fusion Based on Spectral Unmixing

Qi Wei, Simon Godsill, José M. Bioucas-Dias, Nicolas Dobigeon, Jean-Yves Tourneret

19th International Conference on Information Fusion
Heidelberg, Germany - July 5-8, 2016

High-resolution Hyperspectral Image Fusion Based on Spectral Unmixing

Qi Wei, Simon Godsill
Department of Engineering
University of Cambridge
Cambridge, UK CB21PZ
Email:{qi.wei, sjg}@eng.cam.ac.uk

José M. Bioucas-Dias
Instituto de Telecomunicações
Universidade de Lisboa
Lisboa, Portugal 1049-001
Email: bioucas@lx.it.pt

Nicolas Dobigeon, Jean-Yves Tourneret
IRIT/INP-ENSEEIHT
Université de Toulouse
Toulouse, France 31071
Email:{dobigeon, jyt}@n7.fr

***Abstract*—This paper presents a high-resolution hyperspectral image fusion algorithm based on spectral unmixing. The widely used linear observation model (with additive Gaussian noise) is combined with the linear spectral mixture model to form the data terms. The non-negativity and sum-to-one constraints, resulting from the intrinsic physical properties of the abundances (i.e., fractions of the materials contained in each pixel), are introduced to regularize the ill-posed image fusion problem. The joint fusion and unmixing problem is formulated as the minimization of a cost function with respect to the mixing matrix (which contains the spectral signatures of the pure material, referred to as endmembers) , and the abundance maps, with non-negativity and sum-to-one constraints. This optimization problem is attacked with an alternating optimization strategy. The two resulting sub-problems are convex and are solved efficiently using the alternating direction method of multipliers. Simulation results, including comparisons with the state-of-the-art, document the effectiveness and competitiveness of the proposed unmixing based fusion algorithm.**

***Index Terms*—Multi-band image fusion, Bayesian estimation, block circulant matrix, Sylvester equation, alternating direction method of multipliers, block coordinate descent.**

I. Introduction

Hyperspectral (HS) images contain a large number of spectral bands (often of the order of hundreds), which enables fine spectroscopy analysis of the materials present in the analyzed scene. However, owing to physical constrains linked with the available energy to form the images, a high spectral resolution often implies a low spatial resolution.

HS image fusion is a class of inverse problems aimed at enhancing the resolution of the observed images. HS fusion usually involves an observed HS image with high-spectral and low-spatial resolution and a multispectral (MS) image with low-spectral and high-spatial resolution. Note that pansharpening is a similar inverse problem where the HS and MS images are replaced by MS and panchromatic (PAN) images. Inverse problems considered for HS and MS image fusion are often ill-posed and large scale, thus calling for effective regularizers and inference algorithms [1]–[5].

This work was supported by DSO Singapore, and in part by the HYPANEMA ANR Project under Grant ANR-12-BS03-003, and the Thematic Trimester on Image Processing of the CIMI Labex, Toulouse, France, under Grant ANR-11-LABX-0040-CIMI within the Program ANR-11-IDEX-0002-02. Part of this work has been funded thanks to the ERA-NET MED MapInvPlnt Project no. ANR-15-NMED-0002-02.

In general, the degradation mechanisms in HS, MS, and PAN imaging, with respect to (w.r.t.) the target high-spatial and high-spectral image, can be summarized as spatial and spectral linear operations plus additive noise. The HS or MS image fusion is thus often formulated as a regularized linear inverse problem [3]–[5]. Regarding regularization, the usual very high spectral and spatial correlations of the target images imply that they admit sparse or low rank representations, which has been exploited in, for example, [3]–[10].

In [7], a maximum a posteriori (MAP) estimator incorporating a stochastic mixing model has been designed for the fusion of HS and MS images. In [11], a non-negative sparsity constrained algorithm for fusing HS and red-green-blue (RGB) images has been developed based on an alternating optimization method. However, the approaches developed in [7] and [11] assume that the pixels of the low-spatial resolution image are obtained by averaging the high resolution pixels belonging to the same area. The size of the blurring kernel is smaller or equal to the downsampling ratio. This assumption is convenient as it allows the fusion of the two multi-band images to be divided into the fusion of small blocks, which greatly decreases the complexity of the overall problem.[1] However, this assumption is often violated as the size of a blurring kernel can be larger than the downsampling ratio and does not consist of simple uniform averaging.

To overcome the limitations described above, a more general forward model, which formulates blurring and downsampling as two separate operations, has been recently developed [2], [3], [5], [8], [14]–[16]. Based on this model, a non-negative matrix factorization (NMF) method for the fusion of MS and HS images has been proposed in [14]. Similar works have been developed independently in [9], [17]. Later, Yokoya *et al.* have proposed a coupled nonnegative matrix factorization (CNMF) unmixing for fusing low-spatial-resolution HS and high-spatial-resolution MS data, where both HS and MS images are alternately unmixed into endmember and abundance matrices by the CNMF algorithm [8]. This algorithm relies on a physical rationale and is easy to implement owing to its simple update rules. It does not use, however, the abundances estimated from the HS image and the endmember signatures

[1]Note that this assumption has also been used in [10], [12], [13].

estimated from the MS image. Therefore, the spectral and spatial information present in both images is not fully exploited. Besides, the convergence of the CNMF to a stationary point of its cost function is not guaranteed. It is worthy to note that a similar fusion and unmixing framework was recently introduced in [18], in which the alternating NMF steps in CNMF were replaced by alternating proximal forward-backward steps.

In this work, we formulate the HS image fusion as an inverse problem in which the regularization is implicitly imposed by low rank representation inherent to the linear spectral mixture model. In the proposed approach, the endmember signatures and abundances are jointly estimated from the observed multi-band images (i.e., HS and MS images). The optimizations w.r.t. the endmember signatures and the abundances are solved efficiently by the alternating direction method of multipliers (ADMM).

II. Problem Formulation

A. Composite Fusion Model

Combining the widely used linear mixture model [19] and the forward model [2], [20], [21] leads to

$$\begin{aligned} \mathbf{Y}_{\mathrm{M}} &= \mathbf{RMA} + \mathbf{N}_{\mathrm{M}} \\ \mathbf{Y}_{\mathrm{H}} &= \mathbf{MABS} + \mathbf{N}_{\mathrm{H}} \end{aligned} \tag{1}$$

where

- $\mathbf{M} \in \mathbb{R}^{m_\lambda \times p}$ is the endmember matrix whose columns are spectral signatures,
- $\mathbf{A} \in \mathbb{R}^{p \times n}$ is the corresponding abundance matrix whose columns are abundance fractions,
- $\mathbf{Y}_{\mathrm{M}} \in \mathbb{R}^{n_\lambda \times n}$ and $\mathbf{Y}_{\mathrm{H}} \in \mathbb{R}^{m_\lambda \times m}$ are the observed spectrally degraded and spatially degraded images,
- $\mathbf{R} \in \mathbb{R}^{n_\lambda \times m_\lambda}$ is the spectral response of the MS sensor, which can be *a priori* known or estimated by cross-calibration [22],
- $\mathbf{B} \in \mathbb{R}^{n \times n}$ is a cyclic convolution operator acting on the bands,
- $\mathbf{S} \in \mathbb{R}^{n \times m}$ is a $d = d_r \times d_c$ uniform downsampling operator, where d_r and d_c are the row and column downsampling factors, respectively. Therefore, $\mathbf{S}$ has $m = n/d$ ones and zeros elsewhere, which satisfies $\mathbf{S}^T\mathbf{S} = \mathbf{I}_m$,
- $\mathbf{N}_{\mathrm{M}}$ and $\mathbf{N}_{\mathrm{H}}$ are additive Gaussian terms that include both modeling errors and sensor noise.

B. Statistical and variational methods

To summarize, the problem of fusing and unmixing high-spectral and high-spatial resolution images can be formulated as that of estimating the unknown matrices $\mathbf{M}$ and $\mathbf{A}$ from (1), which can be regarded as a joint NMF problem. As it is well known, the NMF problem is non-convex and has no unique solution, leading to an ill-posed problem. The conditioning of this problem is improved by incorporating constraints related to the abundances (matrix $\mathbf{A}$) and the endmembers (matrix $\mathbf{M}$).

Solving the constrained optimization problem including a data-fitting term derived from model (1) is a challenging task, mainly due to the large size of $\mathbf{A}$ and to the presence of the downsampling operator $\mathbf{S}$, which prevents any direct use of the Fourier transform to diagonalize the whole spatial degradation operator $\mathbf{BS}$. To overcome these hurdles, several computational strategies have been proposed including Markov chain Monte Carlo (MCMC) algorithm [3], block coordinate descent method (BCD) [23], and tailored variable splitting, under the ADMM framework [5]. These strategies have been applied to different kinds of regularizations (or priors in the Bayesian framework), e.g., the empirical Gaussian prior [3], [23], sparse regularization [4], or total variation regularization [5].

Recently, contrary to the algorithms described above, a much more efficient method from a computational point-of-view, named *Fast fUsion based on Sylvester Equation* (FUSE) has been proposed to solve explicitly an underlying Sylvester equation associated with the fusion problem derived from (1) [24], [25]. In our work, we regularize this ill-posed problem by exploiting the physical properties of abundances and endmembers, which have been widely used in spectral unmixing, to infer $\mathbf{A}$ and $\mathbf{M}$ from the observed data $\mathbf{Y}_{\mathrm{M}}$ and $\mathbf{Y}_{\mathrm{H}}$.

C. Data Fidelity Term

From the observation model (1) and the assumption that the noise has Gaussian distribution, we adopt the data-fitting term

$$\begin{aligned} &d(\mathbf{M}, \mathbf{A}) = \\ &\frac{1}{2}\|\mathbf{\Lambda}_{\mathrm{H}}^{-\frac{1}{2}}\left(\mathbf{Y}_{\mathrm{H}} - \mathbf{MABS}\right)\|_F^2 + \frac{1}{2}\|\mathbf{\Lambda}_{\mathrm{M}}^{-\frac{1}{2}}\left(\mathbf{Y}_{\mathrm{M}} - \mathbf{RMA}\right)\|_F^2 \end{aligned} \tag{2}$$

where $\mathbf{\Lambda}_{\mathrm{H}}$ and $\mathbf{\Lambda}_{\mathrm{M}}$ denote the covariance matrices of the columns of $\mathbf{N}_{\mathrm{H}}$ and $\mathbf{N}_{\mathrm{M}}$ and it is assumed that both noises are pixel-wise independent.

D. Constraints

1) Abundances: Let $\boldsymbol{a}_j$ and $a_{i,j}$ denote the jth column of $\mathbf{A}$ (associated with the jth image pixel), and the ith component of $\boldsymbol{a}_j$ (representing the proportion of the ith endmember in the jth pixel), respectively. As $a_{i,j}$ represents a proportion [19], [26], then the abundance vectors $\boldsymbol{a}_j$ satisfies the so-called *abundance non-negativity constraint* (ANC) and *abundance sum-to-one constraint* (ASC)

$$\boldsymbol{a}_j \geq 0 \quad \text{and} \quad \mathbf{1}_p^T\boldsymbol{a}_j = 1, \forall j \in \{1, \cdots, n\} \tag{3}$$

where $\geq$ means "element-wise greater or equal than" (for vectors and matrices) and $\mathbf{1}_p$ is a $p \times 1$ vector with all ones. The constraints (3) can be rewritten in matrix form

$$\mathbf{A} \geq 0 \quad \text{and} \quad \mathbf{1}_p^T\mathbf{A} = \mathbf{1}_n^T. \tag{4}$$

2) Endmembers: As the endmember signatures represent the reflectances of different materials, each element of the matrix $\mathbf{M}$ should be between 0 and 1. Thus, the constraints for $\mathbf{M}$ can be written as

$$0 \leq \mathbf{M} \leq 1. \tag{5}$$

E. Constrained Optimization Formulation

By combining the data terms (2) and the constraints (4) and (5), the unmixing based fusion problem can be formulated as the following minimization problem

$$\min_{\mathbf{M},\mathbf{A}} L(\mathbf{M},\mathbf{A}) \quad \text{s.t.} \quad \mathbf{A} \geq 0 \quad \text{and} \quad \mathbf{1}_p^T\mathbf{A} = \mathbf{1}_n^T \\ 0 \leq \mathbf{M} \leq 1 \tag{6}$$

where

$$L(\mathbf{M},\mathbf{A}) = \frac{1}{2}\|\mathbf{\Lambda}_{\mathrm{H}}^{-\frac{1}{2}}\left(\mathbf{Y}_{\mathrm{H}} - \mathbf{MABS}\right)\|_F^2 \\ + \frac{1}{2}\|\mathbf{\Lambda}_{\mathrm{M}}^{-\frac{1}{2}}\left(\mathbf{Y}_{\mathrm{M}} - \mathbf{RMA}\right)\|_F^2.$$

We remark that the inclusion of the covariance matrices $\mathbf{\Lambda}_{\mathrm{H}}$ and $\mathbf{\Lambda}_{\mathrm{M}}$ allows to deal with colored noises (band-dependent), which is often the case in real world applications.

In the proposed formulation, fusion can be regarded as a generalized unmixing problem, which includes two data fidelity terms. Thus, both images contribute to the estimation of the endmember signatures (endmember extraction step) and the high-resolution abundance maps (inversion step). For the endmember estimation, a popular strategy is to use subspace projection as a preprocessing step, such as in [27], [28]. In general, the subspace transformation is learned beforehand from the high-spectral resolution image empirically, e.g., from the HS data. The subspace projection step alleviates the computational burden greatly and can be incorporated in our framework easily.

III. Alternating Optimization Scheme

Even though problem (6) is convex w.r.t. $\mathbf{M}$ and $\mathbf{A}$ separately, it is non-convex w.r.t. these two matrices jointly and thus hard to solve. We attack this hurdle with alternating optimization, also known as block coordinate descent (BCD), w.r.t. $\mathbf{M}$ and $\mathbf{A}$. The optimization w.r.t. $\mathbf{M}$ (resp. $\mathbf{A}$) conditional on $\mathbf{A}$ (resp. $\mathbf{M}$) can be carried out efficiently with the ADMM [29]. Under mild conditions the sequence generated by ADMM converges to a solution of the sub-problem under consideration. The resulting alternating optimization algorithm, referred to as *Fusion based on Unmixing for Multi-band Images* (FUMI), is detailed in Algo. 1, where $\mathrm{EEA}(\mathbf{Y}_{\mathrm{H}})$ in line 1 represents an endmember extraction algorithm to estimate endmembers from HS data, $\mathcal{A} = \{\mathbf{A} \in \mathbb{R}^{p\times n} | \mathbf{A} \geq 0, \mathbf{1}_p^T\mathbf{A} = \mathbf{1}_n^T\}$ is the constraint set associated with ANC and ASC. The optimization steps w.r.t. $\mathbf{A}$ and $\mathbf{M}$ are sketched below. More details about the used optimization strategy are available in [30] and are omitted here for space limitations.

A. Optimization w.r.t. the Abundance Matrix $\mathbf{A}$ ($\mathbf{M}$ fixed)

Let $L(\mathbf{A})$ denote $L(\mathbf{M},\mathbf{A})$ with $\mathbf{M}$ fixed. The optimization w.r.t $\mathbf{A}$ can be formulated as

$$\min_{\mathbf{A}} L(\mathbf{A}) + \iota_{\mathcal{A}}(\mathbf{A}) \tag{7}$$

where

$$\iota_{\mathcal{A}}(\mathbf{A}) = \begin{cases} 0 & \text{if } \mathbf{A} \in \mathcal{A} \\ +\infty & \text{otherwise.} \end{cases}$$

Algorithm 1: Fusion based on Unmixing for Multi-band Images (FUMI)

Input: $\mathbf{Y}_{\mathrm{M}}$, $\mathbf{Y}_{\mathrm{H}}$, $\mathbf{\Lambda}_{\mathrm{M}}$, $\mathbf{\Lambda}_{\mathrm{H}}$, $\mathbf{R}$, $\mathbf{B}$, $\mathbf{S}$

`/* Initialize` $\mathbf{M}$ `*/`

1 $\mathbf{M}^{(0)} \leftarrow \mathrm{EEA}(\mathbf{Y}_{\mathrm{H}})$;

2 **for** $t = 1, 2, \ldots$ **to** *stopping rule* **do**

`/* Optimize w.r.t.` $\mathbf{A}$ `by ADMM */`

3 $\mathbf{A}^{(t)} \in \arg\min_{\mathbf{A}\in\mathcal{A}} L(\mathbf{M}^{(t-1)},\mathbf{A})$;

`/* Optimize w.r.t.` $\mathbf{M}$ `by ADMM */`

4 $\mathbf{M}^{(t)} \in \arg\min_{0\leq\mathbf{M}\leq 1} L(\mathbf{M},\mathbf{A}^{(t)})$;

5 **end**

6 Set $\hat{\mathbf{A}} = \mathbf{A}^{(t)}$ and $\hat{\mathbf{M}} = \mathbf{M}^{(t)}$;

Output: $\hat{\mathbf{A}}$ and $\hat{\mathbf{M}}$

A constrained formulation equivalent to (7) and suitable to apply ADMM is

$$\min_{\mathbf{A}} L(\mathbf{A}) + \iota_{\mathcal{A}}(\mathbf{V}) \text{ s.t. } \mathbf{V} = \mathbf{A}. \tag{8}$$

The augmented Lagrangian for (8) is

$$\mathcal{L}(\mathbf{A},\mathbf{V},\mathbf{G}) = \frac{1}{2}\|\mathbf{\Lambda}_{\mathrm{H}}^{-\frac{1}{2}}\left(\mathbf{Y}_{\mathrm{H}} - \mathbf{MABS}\right)\|_F^2 + \iota_{\mathcal{A}}(\mathbf{V}) \\ + \frac{1}{2}\|\mathbf{\Lambda}_{\mathrm{M}}^{-\frac{1}{2}}\left(\mathbf{Y}_{\mathrm{M}} - \mathbf{RMA}\right)\|_F^2 + \frac{\mu}{2}\left\|\mathbf{A} - \mathbf{V} - \mathbf{G}\right\|_F^2 \tag{9}$$

where $\mathbf{G}$ is the scaled Lagrange multipliers (dual variables) and $\mu > 0$ weights the augmented Lagrangian term.

ADMM iteratively optimizes (9) w.r.t $\mathbf{A}$, then w.r.t, $\mathbf{V}$, and then updates the dual variable $\mathbf{G}$ (see [29] for further details).

Functions $L(\mathbf{A})$ and $\iota_{\mathcal{A}}(\mathbf{V})$ are closed, proper, and convex. According to the Eckstein and Bertsekas's Theorem [31, Theorem 8], the convergence to a solution of (7) is guaranteed.

Note that the optimizations w.r.t. $\mathbf{A}$ and $\mathbf{V}$ can both be solved analytically. The minimization of (9) w.r.t. $\mathbf{A}$ amounts to solve a generalized Sylvester linear equation, which, by exploiting the properties of the circulant and downsampling matrices $\mathbf{B}$ and $\mathbf{S}$, has an analytical solution, as demonstrated in [24], [32]. The update of $\mathbf{V}$ is the Euclidean projection of $\mathbf{A} - \mathbf{G}$ onto the canonical simplex $\mathcal{A}$ [33].

B. Optimization w.r.t. the Endmember Matrix $\mathbf{M}$ ($\mathbf{A}$ fixed)

Let $L(\mathbf{M})$ denote $L(\mathbf{M},\mathbf{A})$ with $\mathbf{A}$ fixed. The optimization of $L(\mathbf{M})$ can be rewritten as

$$\min_{\mathbf{M}} L(\mathbf{M}) + \iota_{\mathcal{M}}(\mathbf{M}), \tag{10}$$

where $\mathcal{M} = \{\mathbf{M} \in \mathbb{R}^{m_\lambda \times p} | 0 \leq \mathbf{M} \leq 1\}$. Assuming that $\mathbf{\Lambda}_H^{-\frac{1}{2}}$ is diagonal and has positive diagonal elements, then, (10) is equivalent to

$$\min_{\mathbf{M}} L(\mathbf{M}) + \iota_{\mathcal{M}}(\mathbf{\Lambda}_{\mathrm{H}}^{\frac{1}{2}}\mathbf{T}) \text{ s.t. } \mathbf{M} = \mathbf{\Lambda}_{\mathrm{H}}^{\frac{1}{2}}\mathbf{T}. \tag{11}$$

The augmented Lagrangian for problem (11) is

$$\mathcal{L}(\mathbf{M},\mathbf{T},\mathbf{G}) = L(\mathbf{M}) + \iota_{\mathcal{M}}(\mathbf{\Lambda}_{\mathrm{H}}^{\frac{1}{2}}\mathbf{T}) + \frac{\mu}{2}\left\|\mathbf{\Lambda}_{\mathrm{H}}^{-\frac{1}{2}}\mathbf{M} - \mathbf{T} - \mathbf{G}\right\|_F^2.$$

ADMM iteratively optimizes $\mathcal{L}(\mathbf{M}, \mathbf{T}, \mathbf{G})$ w.r.t $\mathbf{M}$, then w.r.t, $\mathbf{T}$, and then updates the dual variable $\mathbf{G}$. As $L(\mathbf{M})$ and $\iota_{\mathcal{M}}(\mathbf{\Lambda}_{\mathrm{H}}^{\frac{1}{2}}\mathbf{T})$ are closed, proper, and convex functions and $\mathbf{\Lambda}_{\mathrm{H}}^{\frac{1}{2}}$ has full column rank, the ADMM is guaranteed to converge to the solution of (10).

C. Convergence Analysis

Regarding the sequence generated by Algorithm 1, the Proposition 2.7.1 of [34] asserts that its limit points are stationary points of (6) provided that $L(\mathbf{M}, \mathbf{A})$ is continuously differential in $\mathcal{M} \times \mathcal{A}$ and the minima of (7) and (10) are uniquely attained. The former condition raises no problem but the latter cannot be guaranteed. We may however argue that a simple modification of the objective function, consisting in adding the quadratic term $\alpha_1\|\mathbf{A}\|_F^2 + \alpha_2\|\mathbf{M}\|_F^2$, where α_1 and α_2 are very small, ensures that the minima of (7) and (10) are uniquely attained and thus we may invoke that result. In practice, even without including the quadratic terms, we have systematically observed convergence of the optimization variables $\mathbf{A}$ and $\mathbf{M}$.

IV. Experimental results

The proposed unmixing based fusion method is now applied to semi-real HS and high-resolution images. All the algorithms have been implemented in MATLAB R2014A and run on a computer with Intel(R) Core(TM) i7-2600 CPU@3.40GHz and 8GB RAM.

A. Quality Metrics

1) Fusion Quality: To evaluate the quality of the proposed fusion strategy, five image quality measures have been investigated. Referring to [12], [24], [35], we propose to use the restored signal-to-noise ratio (RSNR), the averaged spectral angle mapper (SAM), the universal image quality index (UIQI), the relative dimensionless global error in synthesis (ERGAS) and the degree of distortion (DD) as quantitative measures. The smaller SAM, ERGAS and DD, the better the fusion. The larger RSNR, UIQI, the better the fusion. Note that these quality metrics have been widely used to assess the quality of a reconstructed multi-band image in image restoration, deconvolution, super-resolution and so on [2], [35].

2) Unmixing Quality: In order to analyze the quality of the unmixing results, we consider the normalized mean square error (NMSE) for both endmember and abundance matrices

$$\mathrm{NMSE}_{\mathbf{M}} = \frac{\|\widehat{\mathbf{M}} - \mathbf{M}\|_F^2}{\|\mathbf{M}\|_F^2}, \quad \mathrm{NMSE}_{\mathbf{A}} = \frac{\|\widehat{\mathbf{A}} - \mathbf{A}\|_F^2}{\|\mathbf{A}\|_F^2}.$$

The smaller NMSE, the better the quality of the unmixing. The SAM between the actual and estimated endmembers (different from SAM defined previously for pixel vectors) is a measure of spectral distortion defined as

$$\mathrm{SAM}_{\mathbf{M}}(\boldsymbol{m}_n, \hat{\boldsymbol{m}}_n) = \arccos\left(\frac{\langle \boldsymbol{m}_n, \hat{\boldsymbol{m}}_n \rangle}{\|\boldsymbol{m}_n\|_2 \|\hat{\boldsymbol{m}}_n\|_2}\right).$$

The overall SAM is obtained by averaging the SAMs computed from all endmembers. The value of $\mathrm{SAM}_{\mathbf{M}}$ is expressed in degrees and, given that the components of $\boldsymbol{m}_n$ and $\hat{\boldsymbol{m}}_n$ are nonnegative, thus belongs to $[0, 90]$. The smaller the absolute value of SAM, the less important the spectral distortion.

B. Stopping Rule

In this work, we use the distance of two consecutive objective function values as the stopping rule mainly due to its simplicity, i.e.,

$$\frac{|L(\mathbf{M}^{(t+1)}, \mathbf{A}^{(t+1)}) - L(\mathbf{M}^{(t)}, \mathbf{A}^{(t)})|}{|L(\mathbf{M}^{(t)}, \mathbf{A}^{(t)})|} < \epsilon$$

where ϵ has been fixed to 10^{-4} by cross-validation.

C. Moffett Dataset

In this experiment, the reference HS image has size $100 \times 100 \times 176$ and it was acquired over Moffett field, CA, in 1994 by the JPL/NASA airborne visible/infrared imaging spectrometer (AVIRIS). This image was initially composed of 224 bands that have been reduced to 176 bands after removing the highly noisy bands due to water vapor absorption. A composite color image of the scene of interest is shown in the bottom right of Figs. 1. As there is no ground-truth for the endmembers and abundances of the reference image, we have unmixed this image with an unsupervised unmixing method and reconstructed the reference image $\mathbf{X}$ with the estimated endmembers and abundances, after normalization enforcing ASC. The number of endmembers has been fixed to $p = 3$.

The reference image $\mathbf{X}$ is reconstructed from a coregistered HS and PAN pair of images. The observed HS image $\mathbf{Y}_{\mathrm{H}}$ has been generated by applying a 7×7 Gaussian filter with standard deviation 1.7 and by down-sampling every 4 pixels in both vertical and horizontal directions for each band of $\mathbf{X}$. A PAN image $\mathbf{Y}_{\mathrm{M}}$ has been obtained by averaging the first 50 HS bands. The HS and PAN images are both contaminated by Gaussian noises such that SNR$= 50$dB for all the bands.

To analyze the role of estimating the endmembers, the proposed FUMI algorithm has been implemented in two scenarios: estimating $\mathbf{A}$ with fixed $\mathbf{M}$, referred to as *supervised FUMI* (S-FUMI) and estimating $\mathbf{A}$ and $\mathbf{M}$ jointly, referred to as *unsupervised FUMI* (UnS-FUMI). Note that the fixed matrix $\mathbf{M}$ used for S-FUMI has been chosen as the matrix $\mathbf{M}$ obtained using SISAL [36].

The proposed FUMI (including both S-FUMI and UnS-FUMI) and two other methods studied in [14] and [8] have been implemented to process the two observed images. The fused images are available in Figs. 1. Visually, S-FUMI and UnS-FUMI give better fused images than the other two methods. Furthermore, the quantitative fusion results reported in Table I are consistent with this conclusion as S-FUMI and UnS-FUMI outperform the other two methods for all the fusion metrics. The price to pay with the S-FUMI and UnS-FUMI methods is their larger computational complexity.

The unmixed endmembers and abundance maps are displayed in Figs. 2 and 3. The quantitative unmixing results are reported in Table II. FUMI methods offer competitive endmember estimation and much better abundance estimation

compared with Berne's and Yokoya's methods. It is interesting to note that even if S-FUMI and UnS-FUMI share very similar fusion results, the endmember estimation obtained with UnS-FUMI is much better compared with S-FUMI, which basically uses the endmembers estimated from the HS image. This gives evidence that the estimation of endmembers benefits from being updated jointly with the abundances, thanks to the complementary spectral and spatial information contained in HS and PAN images.

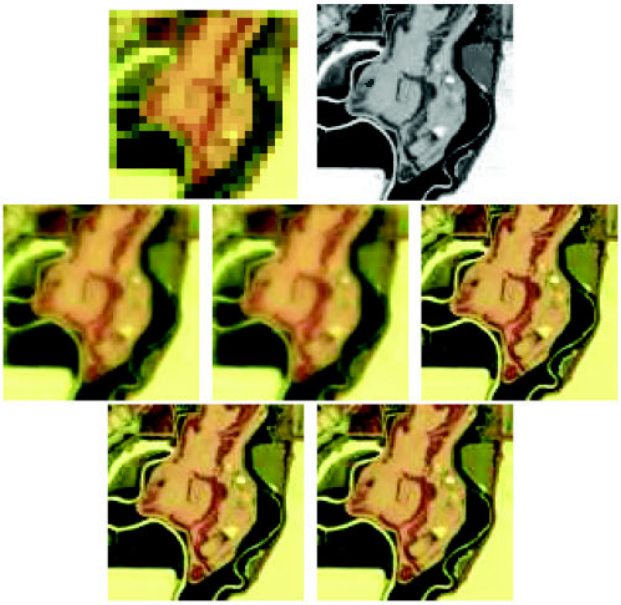

Fig. 1: Fusion results (Moffett datasets): (Top left) HS image. (Top right) PAN image. (Row 2 left) Berne's method. (Row 2 middle) Yokoya's method. (Row 2 right) S-FUMI. (Bottom left) UnS-FUMI. (Bottom right) Reference image.

TABLE I: Fusion Performance for Moffett (HS+PAN datasets): RSNR (in dB), UIQI, SAM (in degree), ERGAS, DD (in 10^{-2}) and time (in second).

Methods	RSNR	UIQI	SAM	ERGAS	DD	Time
Berne2010	16.95	0.8923	4.446	3.777	3.158	0.3
Yokoya2012	17.04	0.9002	4.391	3.734	3.132	1.1
S-FUMI	22.57	0.9799	2.184	2.184	1.488	21.1
UnS-FUMI	22.15	0.9778	2.346	2.292	1.577	32.2

TABLE II: Unmixing Performance for Moffett HS+PAN dataset: SAM_M (in degree), NMSE_M (in dB) and NMSE_A (in dB).

Methods	SAM_M	NMSE_M	NMSE_A
Berne2010	7.568	-16.425	-11.167
Yokoya2012	6.772	-17.405	-11.167
S-FUMI	7.579	-16.419	-14.172
UnS-FUMI	7.028	-16.685	-14.695

V. Conclusion

This paper developed a new algorithm based on spectral unmixing for fusing an hyperspectral image with another high-resolution image. In the proposed algorithm, the endmembers

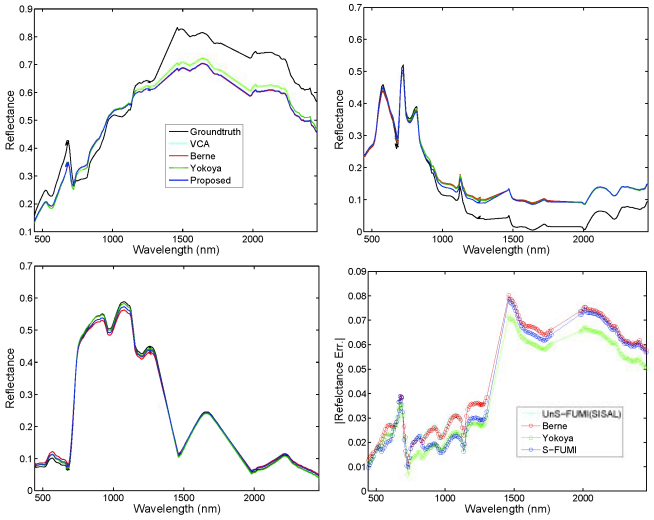

Fig. 2: Unmixed endmembers for Moffett HS+PAN datasets. Top left, top right and bottom left: Actual spectral signatures (ground truth) and estimated endmembers. Bottom right: Sum of absolute values of all endmember errors.

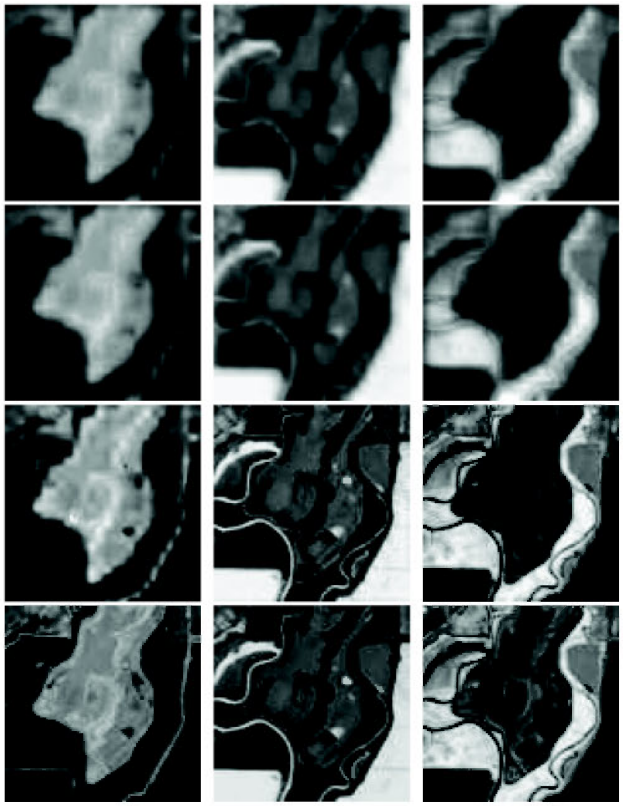

Fig. 3: Unmixed abundance maps for Moffett HS+PAN datasets. Estimated abundance maps using (Row 1) Berne's method, (Row 2) Yokoya's method, and (Row 3) UnS-FUMI. (Row 4) Reference abundance maps.

and abundances were updated alternatively both using an alternating direction method of multipliers. The updates used for the abundances consisted of solving a Sylvester matrix equation and projecting onto a simplex, which were solved analytically and efficiently. The endmember updating was divided into two steps: a least square regression and a thresholding, with light computational cost. Numerical experiments showed that the proposed joint fusion and unmixing algorithm compared competitively with two state-of-the-art methods, with the advantage of improving the performance for both fusion and unmixing.

REFERENCES

[1] B. Aiazzi, L. Alparone, S. Baronti, A. Garzelli, and M. Selva, "25 years of pansharpening: a critical review and new developments," in *Signal and Image Processing for Remote Sensing*, 2nd ed., C. H. Chen, Ed. Boca Raton, FL: CRC Press, 2011, ch. 28, pp. 533–548.

[2] L. Loncan, L. B. Almeida, J. M. Bioucas-Dias, X. Briottet, J. Chanussot, N. Dobigeon, S. Fabre, W. Liao, G. Licciardi, M. Simoes, J.-Y. Tourneret, M. Veganzones, G. Vivone, Q. Wei, and N. Yokoya, "Hyperspectral pansharpening: a review," *IEEE Geosci. Remote Sens. Mag.*, vol. 3, no. 3, pp. 27–46, Sept. 2015.

[3] Q. Wei, N. Dobigeon, and J.-Y. Tourneret, "Bayesian fusion of multi-band images," *IEEE J. Sel. Topics Signal Process.*, vol. 9, no. 6, pp. 1117–1127, Sept. 2015.

[4] Q. Wei, J. Bioucas-Dias, N. Dobigeon, and J. Tourneret, "Hyperspectral and multispectral image fusion based on a sparse representation," *IEEE Trans. Geosci. Remote Sens.*, vol. 53, no. 7, pp. 3658–3668, Jul. 2015.

[5] M. Simoes, J. Bioucas-Dias, L. Almeida, and J. Chanussot, "A convex formulation for hyperspectral image superresolution via subspace-based regularization," *IEEE Trans. Geosci. Remote Sens.*, vol. 53, no. 6, pp. 3373–3388, Jun. 2015.

[6] B. Zhukov, D. Oertel, F. Lanzl, and G. Reinhackel, "Unmixing-based multisensor multiresolution image fusion," *IEEE Trans. Geosci. Remote Sens.*, vol. 37, no. 3, pp. 1212–1226, May 1999.

[7] M. T. Eismann and R. C. Hardie, "Application of the stochastic mixing model to hyperspectral resolution enhancement," *IEEE Trans. Geosci. Remote Sens.*, vol. 42, no. 9, pp. 1924–1933, Sep. 2004.

[8] N. Yokoya, T. Yairi, and A. Iwasaki, "Coupled nonnegative matrix factorization unmixing for hyperspectral and multispectral data fusion," *IEEE Trans. Geosci. Remote Sens.*, vol. 50, no. 2, pp. 528–537, 2012.

[9] Z. An and Z. Shi, "Hyperspectral image fusion by multiplication of spectral constraint and NMF," *Optik-International Journal for Light and Electron Optics*, vol. 125, no. 13, pp. 3150–3158, 2014.

[10] B. Huang, H. Song, H. Cui, J. Peng, and Z. Xu, "Spatial and spectral image fusion using sparse matrix factorization," *IEEE Trans. Geosci. Remote Sens.*, vol. 52, no. 3, pp. 1693–1704, 2014.

[11] E. Wycoff, T.-H. Chan, K. Jia, W.-K. Ma, and Y. Ma, "A non-negative sparse promoting algorithm for high resolution hyperspectral imaging," in *Proc. IEEE Int. Conf. Acoust., Speech, and Signal Processing (ICASSP)*. Vancouver, Canada: IEEE, 2013, pp. 1409–1413.

[12] Y. Zhang, S. De Backer, and P. Scheunders, "Noise-resistant wavelet-based Bayesian fusion of multispectral and hyperspectral images," *IEEE Trans. Geosci. Remote Sens.*, vol. 47, no. 11, pp. 3834 –3843, Nov. 2009.

[13] R. Kawakami, J. Wright, Y.-W. Tai, Y. Matsushita, M. Ben-Ezra, and K. Ikeuchi, "High-resolution hyperspectral imaging via matrix factorization," in *Proc. IEEE Int. Conf. Comp. Vision and Pattern Recognition (CVPR)*. Providence, USA: IEEE, Jun. 2011, pp. 2329–2336.

[14] O. Berne, A. Helens, P. Pilleri, and C. Joblin, "Non-negative matrix factorization pansharpening of hyperspectral data: An application to mid-infrared astronomy," in *Proc. IEEE GRSS Workshop Hyperspectral Image SIgnal Process.: Evolution in Remote Sens. (WHISPERS)*, Reykjavik, Iceland, Jun. 2010, pp. 1–4.

[15] X. He, L. Condat, J. Bioucas-Dias, J. Chanussot, and J. Xia, "A new pansharpening method based on spatial and spectral sparsity priors," *IEEE Trans. Image Process.*, vol. 23, no. 9, pp. 4160–4174, Sep. 2014.

[16] M. A. Veganzones, M. Simões, G. Licciardi, N. Yokoya, J. M. Bioucas-Dias, and J. Chanussot, "Hyperspectral super-resolution of locally low rank images from complementary multisource data," *IEEE Trans. Image Process.*, vol. 25, no. 1, pp. 274–288, Jan 2016.

[17] J. Bieniarz, D. Cerra, J. Avbelj, P. Reinartz, and R. Müller, "Hyperspectral image resolution enhancement based on spectral unmixing and information fusion," in *Proc. ISPRS Hannover Workshop 2011: High-Resolution Earth Imaging for Geospatial Information*, Hannover, Germany, 2011.

[18] C. Lanaras, E. Baltsaias, and K. Schindler, "Advances in hyperspectral and multispectral image fusion and spectral unmixing," *Int. Soc. Photogrammetry Remote Sens.*, vol. XL-3/W3, no. 3, pp. 451–458, 2015.

[19] J. Bioucas-Dias, A. Plaza, N. Dobigeon, M. Parente, Q. Du, P. Gader, and J. Chanussot, "Hyperspectral unmixing overview: Geometrical, statistical, and sparse regression-based approaches," *IEEE J. Sel. Topics Appl. Earth Observ. Remote Sens.*, vol. 5, no. 2, pp. 354–379, Apr. 2012.

[20] I. Amro, J. Mateos, M. Vega, R. Molina, and A. K. Katsaggelos, "A survey of classical methods and new trends in pansharpening of multispectral images," *EURASIP J. Adv. Signal Process.*, vol. 2011, no. 79, pp. 1–22, 2011.

[21] M. González-Audícana, J. L. Saleta, R. G. Catalán, and R. García, "Fusion of multispectral and panchromatic images using improved IHS and PCA mergers based on wavelet decomposition," *IEEE Trans. Geosci. Remote Sens.*, vol. 42, no. 6, pp. 1291–1299, 2004.

[22] N. Yokoya, N. Mayumi, and A. Iwasaki, "Cross-calibration for data fusion of EO-1/Hyperion and Terra/ASTER," *IEEE J. Sel. Topics Appl. Earth Observ. Remote Sens.*, vol. 6, no. 2, pp. 419–426, 2013.

[23] Q. Wei, N. Dobigeon, and J.-Y. Tourneret, "Bayesian fusion of multispectral and hyperspectral images using a block coordinate descent method," in *Proc. IEEE GRSS Workshop Hyperspectral Image SIgnal Process.: Evolution in Remote Sens. (WHISPERS)*, Tokyo, Japan, Jun. 2015.

[24] ——, "Fast fusion of multi-band images based on solving a Sylvester equation," *IEEE Trans. Image Process.*, vol. 24, no. 11, pp. 4109–4121, Nov. 2015.

[25] Q. Wei, N. Dobigeon, J.-Y. Tourneret, J. M. Bioucas-Dias, and S. Godsill, "R-FUSE: Robust fast fusion of multi-band images based on solving a Sylvester equation," submitted. [Online]. Available: http://arxiv.org/abs/1604.01818/

[26] N. Keshava and J. F. Mustard, "Spectral unmixing," *IEEE Signal Process. Mag.*, vol. 19, no. 1, pp. 44–57, Jan. 2002.

[27] J. M. Bioucas-Dias and J. M. Nascimento, "Hyperspectral subspace identification," *IEEE Trans. Geosci. Remote Sens.*, vol. 46, no. 8, pp. 2435–2445, 2008.

[28] N. Dobigeon, S. Moussaoui, M. Coulon, J.-Y. Tourneret, and A. O. Hero, "Joint Bayesian endmember extraction and linear unmixing for hyperspectral imagery," *IEEE Trans. Signal Process.*, vol. 57, no. 11, pp. 4355–4368, 2009.

[29] S. Boyd, N. Parikh, E. Chu, B. Peleato, and J. Eckstein, "Distributed optimization and statistical learning via the alternating direction method of multipliers," *Foundations and Trends® in Machine Learning*, vol. 3, no. 1, pp. 1–122, 2011.

[30] Q. Wei, J. M. Bioucas-Dias, N. Dobigeon, J.-Y. Tourneret, M. Chen, and S. Godsill, "Multi-band image fusion based on spectral unmixing," submitted. [Online]. Available: http://arxiv.org/abs/1603.08720/

[31] J. Eckstein and D. P. Bertsekas, "On the Douglas-Rachford splitting method and the proximal point algorithm for maximal monotone operators," *Mathematical Programming*, vol. 55, no. 1-3, pp. 293–318, 1992.

[32] N. Zhao, Q. Wei, A. Basarab, N. Dobigeon, D. Kouamé, and J.-Y. Tourneret, "Fast single image super-resolution using a new analytical solution for $\ell_2 - \ell_2$ problems," *IEEE Trans. Image Process.*, 2016, to appear. [Online]. Available: http://arxiv.org/abs/1510.00143/

[33] M. Held, P. Wolfe, and H. P. Crowder, "Validation of subgradient optimization," *Mathematical programming*, vol. 6, no. 1, pp. 62–88, 1974.

[34] D. P. Bertsekas, *Nonlinear programming*. Athena Scientific, 1999.

[35] Z. Wang, A. Bovik, H. Sheikh, and E. Simoncelli, "Image quality assessment: from error visibility to structural similarity," *IEEE Trans. Image Process.*, vol. 13, no. 4, pp. 600 –612, Apr. 2004.

[36] J. M. Bioucas-Dias, "A variable splitting augmented Lagrangian approach to linear spectral unmixing," in *Proc. IEEE GRSS Workshop Hyperspectral Image SIgnal Process.: Evolution in Remote Sens. (WHISPERS)*. Grenoble, France: IEEE, Aug. 2009, pp. 1–4.